Isomerization of cyanopropyne in solid argon

Thomas Custer, Urszula Szczepaniak, Marcin Gronowski, Nathalie Piétri, Isabelle Couturier-Tamburelli, Jean-Claude Guillemin, Michal Turowski, Robert Kolos

Isomerization of cyanopropyne in solid argon†

Thomas Custer, *[a] Urszula Szczepaniak, ‡[ab] Marcin Gronowski, [a] Nathalie Pie´tri,[c] Isabelle Couturier-Tamburelli, [c] Jean-Claude Guillemin, [d] Michał Turowski [a] and Robert Kołos [a]

Cyanopropyne, $CH_3–C\equiv C–CN$, is a simple molecule whose photochemistry is still unexplored. Here we investigate the UV photolysis of this astrophysically significant nitrile trapped in solid argon. The FTIR study was assisted with ^{15}N-isotopic substitution data and with DFT-level computations including the analyses of ground- and excited-state potential energy surfaces. Cyanopropyne was found to decay mainly *via* a two-step isomerization process. Infrared absorption spectra evolved to show signals from allenyl cyanide, $CH_2=C=CH–CN$, which then further convert into propargyl cyanide, $H–C\equiv C–CH_2–CN$. Some evidence for the presence of allenyl isocyanide, propargyl isocyanide, 3-cyanocyclopropene, and 1,2,3-butatrien-1-imine under particular experimental conditions was also observed. Although cyano/isocyano interconversion has been observed during photolysis of other closely related species in solid argon matrices, including $H–C\equiv C–CN$, no evidence could be found for production of 1-isocyano-1-propyne, $CH_3–C\equiv C–NC$ for these experiments.

Introduction

Cyanopropyne (**1**, see Fig. 1 for numbering of species), CH_3C_3N, the methylated derivative of cyanoacetylene, HC_3N, is a constituent of interstellar gas clouds[1,2] and, most likely, of Titan's atmosphere.[3,4] An isomer of cyanopropyne, allenyl cyanide (**2**), was also found in interstellar space in low amounts.[5,6] A number of possible astrochemical pathways for the formation of both **1** and **2** have been proposed including ion-molecule[7–9] and a variety of neutral–neutral reactions.[10–12] Molecules **1** and **2** represent a small fraction of bound isomers on a theoretically derived C_4H_3N potential energy surface (PES),[13] several of which may be formed in various astronomical environments. However, the photochemistry of **1**, has never been experimentally or theoretically studied.

The main purpose of this work is to fill this gap by trapping species **1** in cryogenic argon matrices and detecting the photolysis products with infrared absorption spectroscopy. To understand the observed photochemical transformations, we rely on relative energies and harmonic fundamental vibrational frequencies of

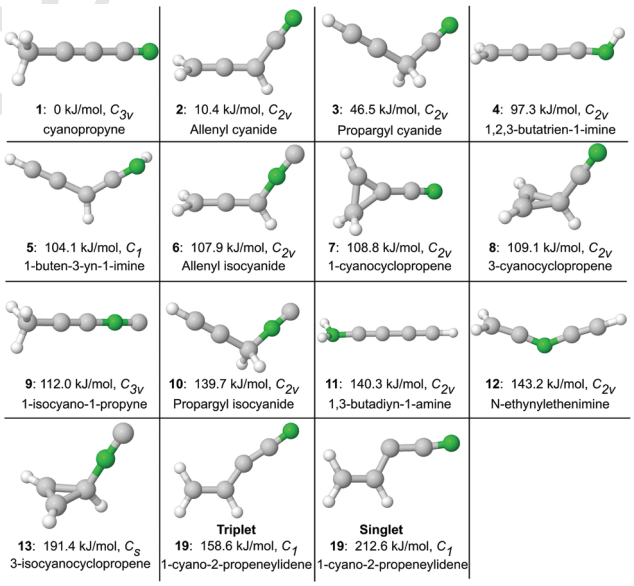

Fig. 1 Ground state geometries of the twelve most stable C_4H_3N molecules at the B3LYP/aug-cc-pVTZ level of theory and three additional isomers pertinent to photochemical transformations described in the text. Electronic energies are relative to species **1**. The triplet ground state and the lowest energy singlet structure are presented for **19**. Reprinted (adapted) with permission from ref. 13. Copyright (2016) American Chemical Society.

[a] *Institute of Physical Chemistry, Polish Academy of Sciences, Kasprzaka 44/52, 01-224 Warsaw, Poland. E-mail: tcuster@ichf.edu.pl*
[b] *Institut des Sciences Moléculaires d'Orsay (ISMO), CNRS, Univ. Paris-Sud, Université Paris-Saclay, F-91405 Orsay, France*
[c] *UMR CNRS 7345, Physique des Interactions Ioniques et Moléculaires, Equipe ASTRO, Aix-Marseille Université, Case 252, Centre de St-Jérôme, 13397 Marseille cedex 20, France*
[d] *Univ. Rennes, Ecole Nationale Supérieure de Chimie de Rennes, CNRS, ISCR-UMR6226, F-35000 Rennes, France*

† Electronic supplementary information (ESI) available. See DOI: 10.1039/c8cp06739b

‡ Current address: IRsweep AG, Laubisruetistrasse 44, 8712 Staefa, Switzerland.

C_4H_3N isomers from our previous study,[13] additional computations for ions, radicals, and transition states connecting various key species, and also the analyses of potential energy surfaces (PESs) pertaining to both ground and excited electronic states. The interpretation of experimental findings was further assisted with the synthesis of four different C_4H_3N isomers in their pure form, and also by ^{15}N isotopic labelling of **1**.

Some experimental studies touching on **1**, **2**, **3**, **6**, **7**, **8**, **9**, and **10** exist to aid in this task. The greatest amount of information is available for **1**. The infrared spectra of **1** in the gas, liquid and solid phases were first reported in 1969.[14] The gas phase values reported in that work were then re-analyzed to include absolute intensities.[15] The IR spectrum was re-measured and new intensities, as well as clear spectra of bands in the far IR, were reported in 1991.[16] Using IR spectroscopy, **1** was detected in an Ar matrix as the primary product of 3-azidopyridazine flash pyrolysis.[17] The IR spectrum of the pure crystalline solid has also been reported.[18]

Less data concerning the IR spectroscopy of species **2** or **3** exists in the literature. In an early synthesis,[19] both **2** and **3** were produced and the IR spectrum of the resulting liquid mixture was reported. This spectrum was measured again in 1970.[20] No complete gas-phase or rare-gas matrix spectrum of either of these chemicals has been published, although select vibrations amongst a mixture of products in an Ar matrix have been given in two different works.[17,20] The situation is similar for **6** and **10**. Here, select vibrational frequencies were published for the neat liquids and for solutions following their synthesis.[21] Recently, the synthetic method was improved[22] and the IR spectra for both **6** and **10**[23] as well as the microwave spectrum of **6**[24] were measured in the gas phase.

Cyano-isocyano conversion is commonly encountered in photolysis experiments where a CN group is present (*e.g.*, HC_3N,[25,26] HC_5N,[27] NC_4N,[28] NC_6N,[29] CH_3CN,[26,30] HCN,[31] C_2H_3CN[32]) and it is reasonable to expect some formation of 1-isocyano-1-propyne (**9**) following photolysis of **1**. Although not synthesized for this work, it has been produced previously *via* flash pyrolysis of an organometallic precursor and its high resolution IR (gas-phase)[33] and microwave[33,34] spectrum measured. A search of the interstellar medium making use of these data[35] did not result in its detection.

The cyclic isomer 3-cyanocyclopropene (**8**) was reportedly produced following pyrolysis of tetrazolo[1.5-*b*]pyridazine and detected in a solution made from the crude pyrolysate following GLC separation.[20] Tentative detection of **7** was also reported in the same work. Isomer **8** has been further described as one component of a mixture of products detected in an Ar matrix following pyrolysis of 3-azidopyridazine as well as photolysis of a mixture of tetrazolo[1.5-*b*]pyridazine and 3-azidopyridazine at 313 nm[17] and in a separate work as a product of photolysis of tetrazolo-[1.5-*b*]pyridazine.[36] A microwave spectrum[37] of this chemical was also collected. A synthetic route to production of 1-cyanocyclopropene (**7**) has been published[38] although it was never isolated in its pure form and no spectra for this species have been measured.

There is precedence to suggest the likely appearance of 1,2,3-butatrien-1-imine (**4**) following photolysis of **1**. These include observation of C_3NH photochemically formed from HC_3N[25] or CH_2CNH from CH_3CN.[26,39–41] However, no experimental measurements of 1,2,3-butatrien-1-imine (**4**) are available. No pertinent spectroscopic studies of other C_4H_3N isomers could be found.

Experimental

Chemicals

Species synthesized include cyanopropyne along with its ^{15}N isotopomer (^{15}N-**1**) and the isomers **2**, **3**, **6**, and **10**. Pertinent synthetic procedures, ^1H and ^{13}C NMR data, and brief comments on handling and purity are given in the Appendix 1 of the ESI.† Although all of these chemicals should be treated with care, particular caution should be used in working with isomers **3** and **6**. At room temperature, both are potentially explosive in their pure form.

Matrix isolation measurements

Complementary photochemical experiments were carried out at the PIIM and IPC PAS, in Marseille and Warsaw, respectively. Distributing measurements between the two laboratories provided access to a broader range of photolyzing UV radiation, critical to differentiating photoproducts and interpretation of the reaction path, as well as information about gas phase absorption intensities used for kinetic analysis and band identification. Examination of the combined data sets also provided a clear view of particular spectral features that are due to disparate matrix microenvironments (matrix ''sites''), only available through experimental repetition. While the equipment used in each laboratory is similar, photolysis capabilities and important details about the experiments differ. At PIIM, sample mixtures with Ar (Linde, 99.99% purity), resulting in a sample : Ar ratio of either 1 : 500 or 1 : 1000 (to assess the influence of complex formation), were made using standard manometric techniques and introduced into a vacuum chamber housing a gold-plated copper support. The support was cooled using a closed cycle helium refrigerator (CTI SC Cryodyne model 21) and the dilute gas mixture deposited on it at a temperature of 20 K and then cooled to 10 K to produce a more transparent ice. Spectra were recorded using an FTIR spectrometer (Nicolet series II Magna System 750) equipped with an MCT detector in the 4000–650 cm^{-1} range. One hundred interferograms were collected for each spectrum with a resolution of 0.125 cm^{-1}. High-energy photolysis experiments were carried out using a microwave discharge hydrogen flow lamp (Opthos Instrument Company, LLC, $\lambda > 121.6$ nm) excited using a McCarrol cavity[42] whose light output passes through a MgF_2 window and impinges on the gold surface in the vacuum of the cryostat chamber. These lamps produce some long wave UV radiation in addition to Ly-α, with the exact output sensitively depending on hydrogen pressure and applied microwave power.[43] The lamp used here was run under conditions maintained as close as possible to those of previous experiments[44] where a total flux of around 5×10^{13} photons cm^{-2} s^{-1} was measured.

At the IPC PAS, gas mixtures of samples with Ar (Multax 99.999%) generally at ratios near 1 : 1000, but also at lower and higher dilution to check for complex formation, were made in a stainless-steel vacuum manifold. A slow flow of the gas mixture was then passed into a vacuum chamber through a microleak valve (Granville-Phillips series 203, Brooks Automation Inc.) and deposited on CsI or sapphire target windows cooled to temperatures ranging from 6 to 25 K using closed cycle helium refrigerators (Advanced Research Systems, Inc. ARS-4HW compressor with DE-202 SE expander or Air Products, Inc. 1R02W-H compressor with Displex DE-202 expander). Different deposition temperatures were used to see their effect on matrix microenvironments. Photolysis was accomplished using an excimer laser (Lambda Physik Compex 102) operating at either 193 nm (ArF) or 248 nm (KrF) with a repetition rate of 10 Hz. The energy per pulse was measured just in front of a quartz vacuum chamber window, normal to the laser beam, using a pyroelectric sensor (Ophir Optronics PE50B). Energies reaching the CsI target just after the quartz window were estimated assuming full illumination of the target, a homogeneous energy distribution across the area of laser beam, and taking into account the 45 degree angle of the target with respect to the incoming light. The evolution of IR absorption spectra was monitored with a Bruker Vertex 70 Fourier transform spectrometer equipped with MCT and combined MCT/InSb detectors with a resolution of 0.16 cm^{-1}. While the number of interferograms collected varied, more than 1024 interferograms were averaged for spectra presented here.

Computational methods

Our prior theoretical study on C_4H_3N isomers[13] has been extended to include shifts in vibrational IR spectra caused by ^{14}N-to-^{15}N isotopic substitution, transition states connecting various low energy isomers, investigation of excited state PESs, as well as calculation of energies and fundamental vibrational frequencies of a number of ions and radicals that might be produced upon photolysis. In order to make these calculations compatible with our previous report,[13] the hybrid B3LYP functional combining Becke's three-parameter exchange contribution[45] with the correlation functional of Lee, Yang, and Parr[46] was employed together with the correlation-consistent polarized valence triple-zeta basis set[47] augmented by diffuse functions (aug-cc-pVTZ). Fundamental harmonic vibrational frequencies were calculated at the same level of theory (B3LYP/aug-cc-pVTZ). These calculations were carried out on a local cluster in the IPC PAS laboratory.

Ground state potential energy surface screening

In order to localize the deepest minima on various ground state PESs (C_4H_4N, $C_4H_4N^+$, C_4H_2N, and $C_4H_2N^-$) we performed a two-step procedure very similar to that described in our previous work.[13] Briefly, a set of 14 unique carbon–nitrogen skeletons is generated which have four carbons and one nitrogen, with each of these atoms occupying positions relative to one another appropriate to sp^3 hybridization. The H atoms are then placed in all possible positions on these skeletons, also with appropriate sp^3 hybridization. Each of these structures were then subjected to geometry optimization at the B3LYP/4-31G level of theory. Various energy cutoff values were used in an attempt to balance the time needed for computation *versus* production of a complete set of isomers. The cutoff values used for this work are: −209.16492 Hartree (~184 kJ mol^{-1} above the global minimum) for C_4H_4N, −208.88667 Hartree (~164 kJ mol^{-1} above the global minimum) for $C_4H_4N^+$, −207.88 Hartree (~262 kJ mol^{-1} above the global minimum) for C_4H_2N, and −207.92 Hartree (~156 kJ mol^{-1} above the global minimum) for $C_4H_2N^-$. Structures having energies lower than a given cutoff value were used as the starting points for more accurate B3LYP/aug-cc-pVTZ optimization and IR frequency determination. Determining IR frequencies at this level of theory provided a good compromise between time and accuracy for the large number of calculations performed. While accounting for anhamonicity and use of more advanced electronic structure methods is possible, significant gains in accuracy would only be achieved at high computational cost.[48] In the case of the $C_4H_3N^+$ PES, optimized structures for the C_4H_3N PES from our previous work,[13] with an electron removed, were used as starting geometries for optimization. Transition states were located using the synchronous transit-guided quasi-Newton (STQN) method,[49,50] as implemented in Gaussian software with the QST2 and QST3 procedures. We applied the QST3 approach only if QST2 failed and the Berny algorithm[51] only if STQN methods failed. The nature of localized transition states was verified both by inspection of vibrational frequencies (exactly one imaginary value) and using intrinsic reaction coordinate (IRC) calculations.[52] These calculations were carried out using the Gaussian 09 Rev. E. 01 or Rev. B. 01 software. Jmol[13] and Gabedit[53] were used in preparation of input and visualization of output data.

Analysis of potential energy surfaces in excited states

In order to describe the mechanism of the photo-induced reaction, knowledge of excited state PESs is crucial. Due to computational demands of these excited state calculations, we used the aug-cc-pVTZ basis set in conjunction with the hybrid meta-GGA correlation functional B1B95.[54] This functional produces acceptable results for conformational energies,[55] barrier heights,[56] excitation energies,[57] and reaction energies.[58] Triplet and singlet excited state calculations were carried out using time-dependent version[59–61] of DFT. The Tamm–Dancoff approximation was applied to provide reliable results for numerically unstable cases.[62–66] Excited state energies relevant to a given isomerization path were calculated assuming vertical excitations for a series of geometries provided by the respective ground state IRC (intrinsic reaction coordinate) calculation. All excited state calculations were carried out using the Gaussian 09 Rev. E. 01 program with preparation of inputs and visualization of outputs using ChemCraft.[67]

Results and discussion

Ground-state PES computations

The UV radiation used in these experiments was provided by λ = 248 nm, λ = 193 nm, and $\lambda > 121.6$ nm sources (482, 620,

and <984 kJ mol^{-1}, respectively). Our initial quantum chemical study involved only the ground electronic state PES and was useful in ascertaining what potential photolysis products could be neglected in further considerations. This was divided into several categories, dealing with isomers, products of ionization, homo- or heterolytic bond cleavages, and hydrogen addition. Relevant structures, energies, vibrational frequencies and IR absorption intensities for the optimized lowest energy members of the $C_4H_3N^+$, $C_4H_2N^-$, C_4H_2N, and C_4H_4N families of isomers, greatly expanding on C_4H_3N molecules reported previously,[13] are provided in Appendix 2 of the ESI† (Fig. S4–S8 and Tables S2–S11, ESI†). Energetics of transition states connecting C_4H_3N isomers were also calculated and can be found in Fig. S1–S3 of the ESI.† IR band frequency and intensity shifts expected due to ^{15}N substitution in C_4H_3N isomers are given in Tables S12–S23 of the ESI.†

Scheme 1 combines insights from this theoretical analysis and literature, constrained by our experimental results reported in the following sections. Ground state calculations suggest the feasibility of isomerization induced by $\lambda > 121.6$ nm photons, either *via* H atom migration or movement of the CN group. Homolytic C–H bond cleavage should also be possible and could result in formation of a variety of C_4H_2N radicals upon escape of H from the matrix cage. The most likely to be formed are those involving the loss of H from **1**, **2** or **3** (Fig. S7 and Tables S6, S7, ESI†). Further dehydrogenation would lead to formation of species from the C_4HN or C_4N families.[68] Escape of an H atom from the matrix cage may give rise to production of C_4H_4N radicals (the most stable being those formed *via* addition of H to the double bond of **2**, Fig. S8 and Tables S10, S11, ESI†). Although homolytic C–C or C–N bond cleavage might be favored in the gas phase, in a matrix it will likely result in simple isomerization (Table S1, ESI†). Few or no ionic products are expected to be observed upon photolysis (Fig. S5, S6 and Tables S4, S5, S8, S9, ESI†). The most likely charged products would be molecular cations (Fig. S4 and Tables S2, S3, ESI;† species $\mathbf{4}^+$ is predicted to be the most stable of these) formed at $\lambda > 121.6$ nm or due to two-photon processes.

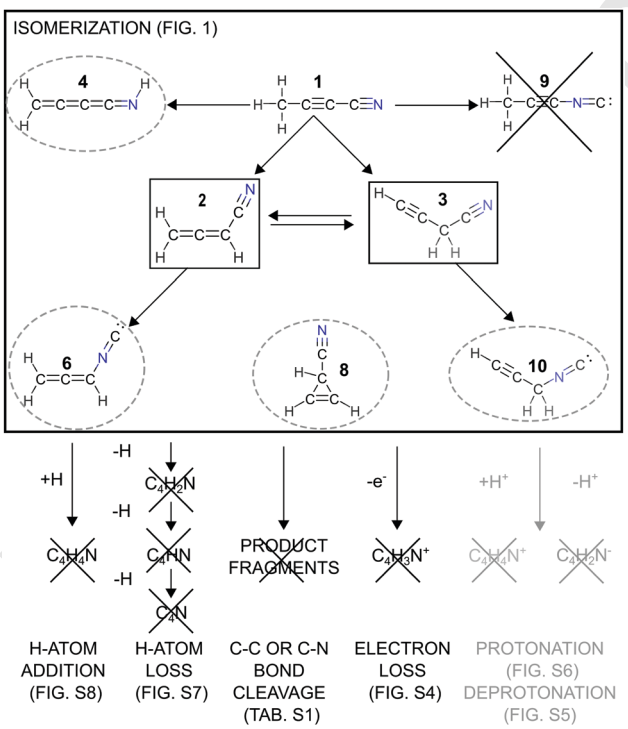

Scheme 1 Summary of cyanopropyne photolysis products ($\lambda > 121.6$ nm). Reactions deemed unlikely according to ground state PES calculations are marked in grey. Unobserved species (see the 'Photoproduct spectra' section) are crossed out. The detection of isomers distinguished by a solid square (detected) and a dashed circle (tentative).

Photoproduct spectra

When matrix-isolated species **1** (see Table 1 for IR absorption features) is irradiated using an ArF or KrF excimer laser or a hydrogen discharge lamp, the IR bands of the parent decrease and new bands appear. While the main photoproducts, **2** and **3**, could be unambiguously identified by comparison to the spectra of pure chemicals isolated in Ar matrices, the agreement with reference data was seldom exact (*cf.* Tables 2, 3 and Fig. 2, 3). A matrix cage well suited to a precursor species may not easily accommodate a particular photogenerated isomer. Consequently, vibrational motion of the photoproduct can be constrained, causing deviations from anticipated frequencies and alteration of the IR band intensity pattern.[69] While frequency deviations, when present, were on the order of several wavenumbers, the intensity changes could be substantial. Still, the most intense of the expected fundamental bands remained strong and those predicted as the weakest were difficult to detect. Variation in intensity can be seen by comparing relative peak heights from one column to the next in Fig. 2–4. As a rule, intensity patterns observed within the site-induced multiplets of product species were not reproduced in reference spectra, even though the frequencies of some multiplet components could be conserved. Spectral attributions were assisted by the application of ^{15}N-labeled precursor (**1**) molecules (Tables 2 and 3).

Further support for the identification of isomers **2** and **3** was provided by the analysis of integrated band intensities plotted as a function of irradiation time. Bands originating in the same carrier shared common growth/decay patterns. Detailed remarks pertaining to our analysis of all photoproduct spectra can be found in Appendix 3 of the ESI.†

Isocyanides 6 and 10. It is difficult to prove formation of either allenyl isocyanide (**6**) or propargyl isocyanide (**10**) unambiguously from these experiments. In the case of **6**, three candidate spectral features were picked up based on the comparison of the photolysed ($\lambda > 121.6$ nm) matrix to the sample of authentic Ar matrix-isolated compound and on the predicted ^{14}N–^{15}N isotopic shifts (Fig. 4 and Table 4). Two of the proposed bands are very near the signal-to-noise limit, excluding any reliable analysis of their evolution throughout the photolysis.

Even less certain is the identification of **10** (see Table S24 and Fig. S33–S44, ESI†). This hinges on one band, 2160 cm^{-1}, which appears upon either hydrogen lamp or ArF laser photolysis. This feature exhibits a ^{14}N–^{15}N isotope frequency shift very close to the predicted value (observed -39 cm^{-1} *vs.*

Table 1 Main IR absorption bands for cyanopropyne (**1**) as theoretically predicted (harmonic approximation, frequencies scaled by 0.96) and experimentally observed. Relative intensities are given in parentheses. Ranges generally indicate the most intense features of a multiplet with possible weak features falling outside the range

	Calculation			Experiment						
	B3LYP/aug-cc-pVTZ vibrational frequency in cm^{-1} (relative IR intensity)			Experimental frequency in cm^{-1} (relative IR intensity)						
				Literature				This work		
	Literature[13]	This work		Gas-phase[14]	Gas-phase[16]	Crystalline[18]	Ar matrix[17]	Ar matrix	Ar matrix	Shift
	^{14}N[a]	^{15}N	^{14}N–^{15}N freq. shift	^{14}N	^{14}N[b]	^{14}N[c]	^{14}N	^{14}N	^{15}N	^{14}N–^{15}N freq. shift
ν_2	2295 (100)	2287	−8	2277–2265 (vs)	2279–2268 (100)	2275 (100)	2274 (s)	2284–2271 (100)	2275–2262 (100)	−9
$2\nu_5$				2320 (vs)	2341–2332 (118)	2339 (74)		2346–2333 (45)	2337–2325 (80)	−9
ν_8	1410 (7)	1410	0	1445 (s)	1454 (64)	1435, 1414, 1407 (67)	1415 (m)	1437 (25)	1437 (23)	0
ν_1	2909 (4)	2909	0	2944–2933 (m)	2944–2909	2926, 2908 (3)		2934 (<1)	2934 (<1)	0
ν_{10}	524 (3)	523	−2	499 (vs)	500 (21)	505 (15)	505 (w)	504–499 (16)	502–498 (22)	−2
ν_9	1007 (1)	1007	0	1030 (m)	1031 (9)	1020, 1016 (8)	1027 (w)	1027–1025 (8)	1027–1025 (7)	0

[a] Relative to ν_2 with a value of 135 km mol^{-1}. [b] Relative to ν_2 with a value of 23.63 km mol^{-1}. [c] Relative values of integrated absorption coefficient at 35 K relative to ν_2 which has a value of 1.2×10^5 cm^{-2}.

Table 2 Main IR absorption bands for allenyl cyanide (**2**) as theoretically predicted (harmonic approximation, frequencies scaled by 0.96) and experimentally observed. Relative intensities are given in parentheses. See Fig. 2 and ESI for detailed spectra

	Calculation			Experiment				
	B3LYP/aug-cc-pVTZ vibrational frequency in cm^{-1} (relative IR intensity)			Experimental frequency in cm^{-1} (relative IR intensity)				
				Literature	This work			
	Literature[13]	This work		Ar matrix[17]	Ar matrix	Ar matrix from $CH_3C_3{}^{14}N$ phot.	Ar matrix from $CH_3C_3{}^{15}N$ phot.	
	^{14}N[a]	^{15}N	^{14}N–^{15}N freq. shift	^{14}N	^{14}N	^{14}N	^{15}N	^{14}N–^{15}N freq. shift
ν_4	1959 (100)	1959	0	1976 (s)	1982–1978 (100)	1986–1978	1985–1978	<1
ν_9	862 (50)	862	0	858 (s)	858–851 (80)	858	858	0
ν_3	2241 (26)	2213	−28	2227(m)	2233–2224 (7)	2228–2225	2203	−25
ν_{15}	840 (25)	840	0	843/839 (m)	838–834 (24)	836–834	836–834	<1
ν_8	912 (9)	908	−5		924–914 (23)	918–914	915–910	−3, −4
ν_5	1405 (4)	1405	0		1417–1415 (12)	1417–1415[b]	1417–1415[b]	<1

[a] Relative to ν_4 with a value of 92 km mol^{-1}. [b] Contributions to this band from both **2** and **3**.

−37 cm^{-1} theoretical) and is expected to be the strongest IR feature of this isomer.

No evidence for isocyanopropyne 9. Chemical intuition might lead one to expect formation of species **9**, a product potentially arising *via* simple cyano/isocyano conversion of cyanopropyne, **1**. However, no experimental evidence was found for its formation here. Gas-phase vibrational frequencies are available for **9** in the literature[33] which, in conjunction with the theoretical predictions, help to constrain expected frequencies in a matrix (Fig. S52–S57, ESI†). While a number of candidates might be postulated for the strongest IR band of **9**, all falling within 10 cm^{-1} of its measured gas-phase band center (2083 cm^{-1}), it is impossible to unambiguously associate any one of these with a ^{15}N partner having a shift of −35 cm^{-1}.

Imine 4. According to calculations, isomer **4**, 1,2,3-butatrien-1-imine (CH_2CCCNH), is more stable than any of the three lowest-energy C_4H_3N isocyanides (Fig. 1). Evidence for production of **4** consists of a shoulder on the peak at 2160 cm^{-1} (see Fig. S34, S45, and S46, ESI†) which may belong to the most intense IR feature of this molecule (predicted intensity over 1400 km mol^{-1}). A candidate for the corresponding ^{15}N-band appears with a correct spectral shift: −3.1 cm^{-1} (prediction: −3 cm^{-1}). There is no good evidence for any of the other bands of isomer **4** which are expected to be at least several times weaker, making this attribution very tentative.

Cyclic isomer 8. Finally, the cyclic species 3-cyanocyclopropene (**8**) should be considered as a potential, if not probable, product. At all irradiation wavelengths, a feature at 986 cm^{-1} could be found. It is the same location as previously reported[17] for the second most intense IR band of **8** in solid Ar (Fig. S33 and S58–S63, ESI†). The strongest IR absorption was expected at 624 or 623 cm^{-1} (out of range for hydrogen lamp photolysis experiments), and it became visible at 623 cm^{-1}, albeit weakly, following our 248 nm irradiations. The ^{14}N-to-^{15}N frequency shift of that

Table 3 Main IR absorption bands for propargyl cyanide (**3**) as theoretically predicted (harmonic approximation, frequencies scaled by 0.96) and experimentally observed. Relative intensities are given in parentheses. Empty entries indicate bands not detected. See Fig. 3 and ESI for detailed spectra

	Calculation			Experiment				
	B3LYP/aug-cc-pVTZ vibrational frequency in cm^{-1} (relative IR intensity)			Experimental frequency in cm^{-1} (relative IR intensity)				
				Literature	This work			
	Literature[13]	This work		Ar matrix[17]	Ar matrix	Ar matrix from $CH_3C_3{}^{14}N$ phot.	Ar matrix from $CH_3C_3{}^{15}N$ phot.	
	^{14}N[a]	^{15}N	^{14}N–^{15}N freq. shift	^{14}N	^{14}N	^{14}N	^{15}N	^{14}N–^{15}N freq. shift
ν_1	3329 (100)	3329	0	3318 (vs)	3337–3319 (100)	3336–3319	3336–3318	<1
ν_{16}	664 (62)	664	0	624 (m)	649–645 (65)	649–647	649–648	0
ν_9	679 (54)	679	0	659 (s)	663 (60)	662	662	<1
ν_6	1288 (18)	1288	0	1313 (m)	1292–1285 (19)	1289	1289	<1
ν_5	1393 (13)	1393	0	1434 (w)	1417–1413 (23)	1417–1415[c]	1417–1415[c]	<1
ν_8	864 (9)	860	−4		899–885 (9)	896	893	−3
ν_3	2271 (7)	2242	−29		2272 (6)[b]	—[d]	—[d]	
ν_7	952 (7)	950	−2	981 (w)	984–979 (6)			

[a] Relative to ν_1 with a value of 70 km mol^{-1}. [b] ν_3 matrix assignment uncertain. [c] Contribution to this band from both **2** and **3**. [d] The product band is masked by the strong absorption of ν_2 for chemical **1** (for both ^{15}N and ^{14}N).

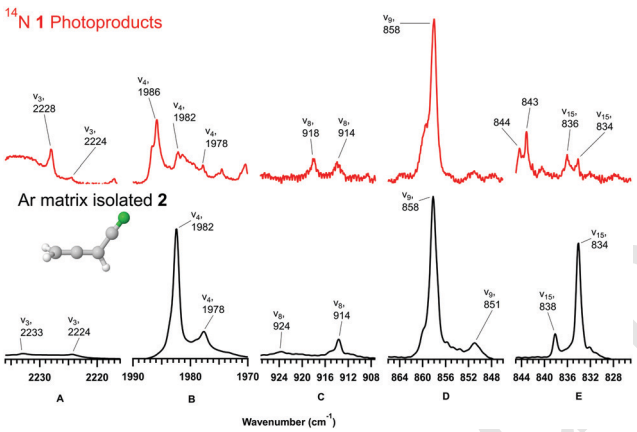

Fig. 2 Top: Difference spectrum showing irradiation of ^{14}N-**1** in an Ar matrix ($\lambda > 121.6$ nm, ~23 h) using the unphotolyzed, freshly deposited ^{14}N-**1** in Ar as background. Bottom: Freshly deposited, Ar matrix isolated **2** for the regions surrounding bands of highest intensity for **2**. Bands assigned to **2** are indicated. Absorbance scales for all columns in a given row are identical to allow direct visual intercomparison of intensities.

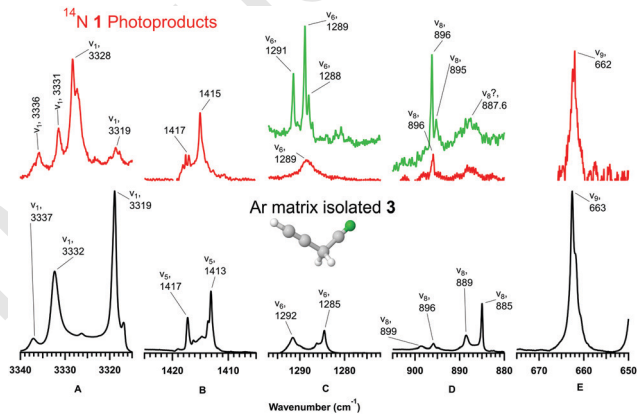

Fig. 3 Top: Difference spectrum showing irradiation of ^{14}N-**1** in an Ar matrix ($\lambda > 121.6$ nm, ~23 h) using the unphotolyzed, freshly deposited **1** in Ar as background. Bottom: Freshly deposited, Ar matrix isolated **3** for the regions surrounding bands of highest intensity for **3** (ν_{16} is out of the measurement range). Green traces in the upper parts of columns C and D are the results of 193 nm irradiation of ^{14}N-**1** provided to show the structure of bands that can sometimes be seen. Bands assigned to **3** are indicated. Absorbance scales for all columns in a given row are identical to allow direct visual intercomparison of intensities.

band, −2 cm^{-1}, closely matched the predicted value of −1.4 cm^{-1}. No isotope shift appeared for the 986 cm^{-1} feature, just as predicted by the theory. The low intensities of these bands do not permit analysis of their correlation and therefore prevent any dependable conclusion as to their common origin.

Other products. A thorough search of the experimental data was conducted using theoretical results previously published[13] for 54 C_4H_3N isomers, now extended to include ^{14}N–^{15}N vibrational frequency shifts (see Table S14, ESI†). No matches were found, apart from those reported above. Other plausible closed-shell products for which reliable Ar-matrix values are available in the literature include HCN,[70,71] CH_4,[72] CH_3CCH,[73] HCCH,[74,75] and HC_3N.[25] Of these, there is limited evidence (only one experiment) that HCCH was produced following $\lambda > 121.6$ nm irradiation. Theoretical data exists for C_4HN[76–80] and C_4N,[68] both species that might be expected by analogy to HCCN, CCN, and CNC produced *via* "H-atom stripping" from CH_3CN in an Ar matrix exposed to $\lambda > 121.6$ nm radiation.[30] No convincing matches were found from amongst a selection of 4 potential carbene C_4HN species. Although interesting structures exist in the ranges between 1379–1460 cm^{-1} and 1940–2000 cm^{-1} where intense vibrations for various C_4N species should reside, no reliable identification could be made. A search for CH_3[81–83] and CN[31] radicals did not indicate their production.

Kinetics

The decay of the most intense bands of precursor **1** irradiated with a hydrogen lamp and the time evolution of the resultant

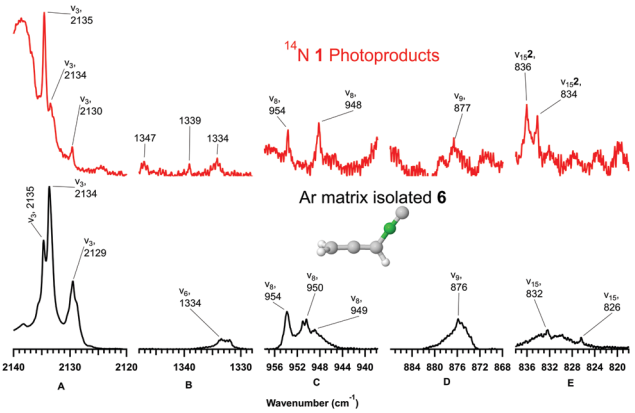

Fig. 4 Top: Difference spectrum showing irradiation of ^{14}N-**1** in an Ar matrix ($\lambda > 121.6$ nm, ~23 h) using the unphotolyzed, freshly deposited **1** in Ar as background. Bottom: Freshly deposited, Ar matrix isolated **6** for the regions surrounding bands of highest intensity for **6**. Bands assigned to species other than **6** are labelled with respective isomer numbers. Absorbance scales for all columns in a given row are identical to allow direct visual intercomparison of intensities.

main photoproducts, **2** and **3**, are plotted in Fig. 5, panel A. Allenyl cyanide (**2**) grows rapidly in the early stages of irradiation, peaks near 250 minutes, and gradually decreases at longer times. Propargyl cyanide (**3**) rises steadily throughout the photolysis while the parent species decreases. Photoproducts **2** and **3** are also potentially subject to secondary photoreactions. To further investigate connections between these species, H_2 lamp photolyses of Ar-matrix isolated **2** (panel B) and a mixture of **2** and **3** (panel C) were also conducted. During the photolysis of isomer **2** we clearly observe the production of **3**. While the strongest band of **3** observed upon irradiation of **1** appears as a matrix site-split doublet (3331.5 and 3328.3 cm^{-1}), the direct photolysis of **2** produces only a single band of **3** in that region (3331.4 cm^{-1}) reflecting shape/size differences between initial matrix cages of the two precursors. Photolysis of **3** together with residual **2** results in a steady decline of both over the course of irradiation. Conversion of **3** to **2** is masked in Fig. 5C by residual **2** but can be recovered from kinetic analysis.

A simple kinetic model was fit to the time evolution of measured molar column densities of **1**, **2**, and **3**. These were calculated using gas-phase absorption intensities at the IPC PAS laboratory (34 km mol^{-1} for ν_2 of **1**, 19 km mol^{-1} for ν_4 of **2**, and 86 km mol^{-1} for ν_1 of **3**) along with the corresponding integrated peak intensities in Ar-matrix spectra coming from our photolysis experiments. While measured gas phase absorption intensities may differ from those of the matrix isolated molecules, these values are the best currently available for this simple analysis. The resulting column densities (moles cm^{-2}) had to be used in lieu of concentrations (moles cm^{-3}) as the matrix thickness was not monitored during these experiments. The kinetic model assumes (i) the possibility of UV-induced transformations between the lowest-energy C_4H_3N isomers **1**, **2**, and **3**, (ii) the decay of these three species due to other, unspecified unimolecular reactions, and (iii) the gradual build-up of atmospheric gases (leaks into the chamber) that inevitably form a layer on top of the matrix and diminish the flux of photolyzing UV radiation reaching the molecules of interest over time. Mathematical expressions for this model are given by the coupled differential eqn (1)–(3):

$$\frac{d[\mathbf{1}]}{dt} = -(k_{1,2} + k_{1,3} + k_1)[\mathbf{1}]e^{-k_{Phot} \times t} \quad (1)$$

$$\frac{d[\mathbf{2}]}{dt} = (k_{1,2}[\mathbf{1}] - (k_{2,3} + k_2)[\mathbf{2}] + k_{3,2}[\mathbf{3}])e^{-k_{Phot} \times t} \quad (2)$$

$$\frac{d[\mathbf{3}]}{dt} = (k_{1,3}[\mathbf{1}] + k_{2,3}[\mathbf{2}] - (k_{3,2} + k_3)[\mathbf{3}])e^{-k_{Phot} \times t} \quad (3)$$

Table 4 Main IR absorption bands for allenyl isocyanide (**6**) as theoretically predicted (harmonic approximation, frequencies scaled by 0.96) and experimentally observed. Relative intensities are given in parentheses when available. Empty entries indicate bands not detected. See Fig. 4 and ESI for detailed spectra

	Calculation			Experiment				
	B3LYP/aug-cc-pVTZ vibrational frequency in cm^{-1} (relative IR intensity)			Experimental frequency in cm^{-1} (relative IR intensity)				
				Literature	This work			
	Literature[13]	This work		Gas[23]	Ar matrix	Ar matrix from $CH_3C_3{}^{14}N$ phot.	Ar matrix from $CH_3C_3{}^{15}N$ phot.	
	^{14}N[a]	^{15}N	^{14}N–^{15}N freq. shift	^{14}N	^{14}N	^{14}N	^{15}N	^{14}N–^{15}N freq. shift
ν_3	2110 (100)	2071	−38	2133	2135–2129 (100)	2135–2130	2097	−37
ν_9	880 (21)	880	0	875	876 (30)	877	877	0
ν_8	929 (14)	926	−3	952	954–949 (37)	954–948	950–946	−3, −2
ν_{15}	838 (11)	838	0	834	832–826 (22)			
ν_6	1314 (9)	1314	−1	1338	1334–1332 (9)			
ν_4	1966 (9)	1966	0	1966	1957 (4.5)[b]			
ν_5	1414 (8)	1414	0	1449	1443 (3)[c]			
ν_{10}	582 (5)	577	−5	593	602–601 (3)			
ν_7	1116 (2)	1116	−1	1126	1122–1119 (4)			

[a] Relative to ν_3 with a calculated value of 193 km mol^{-1}. [b] Assignment tentative. Close coincidence with $\nu_7 + \nu_9$.[23] [c] Assignment tentative. Close coincidence with $\nu_{15} + \nu_{16}$.[23]

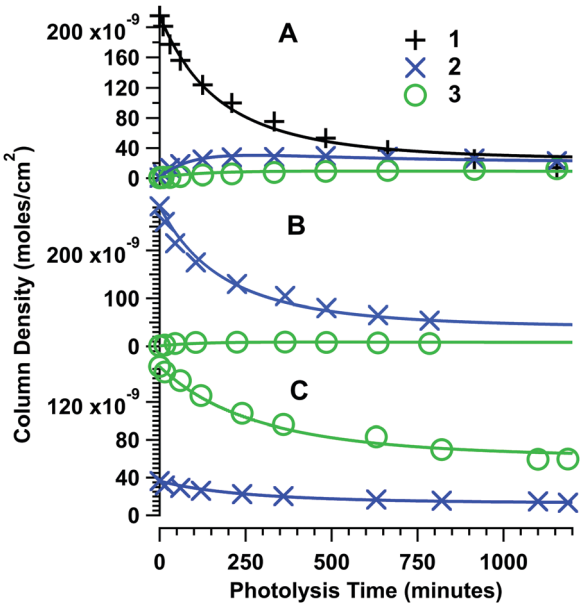

Fig. 5 Cyanopropyne (**1**, black "+" signs), allenyl cyanide (**2**, blue "×"), and propargyl cyanide (**3**, green circles) column densities as a function of time during the hydrogen lamp ($\lambda > 121.6$ nm) irradiation of either **1** isolated in solid argon (panel A), **2** isolated in solid Ar (panel B), or **3** (with a contamination by **2**) isolated in solid Ar (panel C). Solid lines are best fits of experimental data points to the kinetic model (eqn (1)–(3)). Reaction rate coefficients are listed in Table S27 of the ESI.†

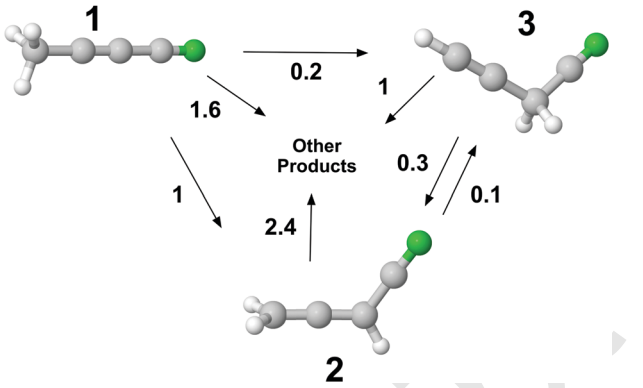

Fig. 6 Schematic showing the relative values of first-order rate constants for photochemical transformations of the three lowest-energy cyanopropyne (**1**) isomers in solid argon, induced with hydrogen lamp radiation ($\lambda > 121.6$ nm). Rate coefficients normalized to that of allenyl cyanide (**2**) production from **1**.

where k_{ij} represents the rate coefficient for a given $i \rightarrow j$ conversion, k_i governs first order decay of isomer i to other products, and k_{Phot} represents a constant UV optical density increase per unit time. A schematic representation of the model is given in Fig. 6. Photolysis experiments starting from **2** or **3** yield only trace amounts of species **1**. This observation is reflected in the model by closing return paths to **1**. Although additional species, in particular **4**, **6**, **8**, and **10** may have been formed, due to uncertainties in identification they are not treated individually but constitute a part of the "other products".

Excited state potential energy surfaces

The most important potential energy surfaces (PES) for these photochemical reactions are those of the lowest excited electronic states (singlet or triplet). These may be reached by fast internal conversion or intersystem crossing processes. The changes of ground- and excited-state energies along the path leading from **1** to **3** are presented in Fig. 7 (columns B to F) along with the transformation from **1** to **9** (column A). Structures sampled from along each of these reaction coordinates are given in Fig. S77–S84 in the ESI.† Gaps between each column are labelled with the appropriate ground-state species where a "T" signifies a triplet and "S" a singlet state. Each of these processes will be addressed in turn.

Isomerization of 1 to 2. In spite of an intense search for a transition state directly linking species **1** and **2**, none was found on the ground-state potential energy surface. After reaching the S_1 or S_2 state of **1** (with likely vibrational excitation), the lowest barrier in the T_1 state (at ~550 kJ mol^{-1}; see Fig. 7, column B) can be overcome to allow access to the transient intermediate **19**, $H_2C{=}CH{-}CCN$, whose ground state is a triplet (see Fig. 1 for its structure). Both H_2 lamp radiation and 193 nm excimer laser radiation have sufficient energy to surmount the barrier while 248 nm excimer laser radiation does not. Nevertheless, measurable amounts of **2** are consistently formed when working with 248 nm radiation (~6 mJ cm^{-2}) while one test using ~0.2 mJ cm^{-2} showed none. This suggests involvement of a two-photon process for this wavelength at higher laser output. Exclusively low power output (~0.3–0.1 mJ cm^{-2}) was used for 193 nm data presented here and the main products resemble those observed using the H_2 discharge light source. Electronic spectra of **1** have already been reported extending from about 244 nm to well under 80 nm.[84,85] For 193 nm radiation, the involved transition is $B^1E \leftarrow X^1A_1$. For far-UV wavelengths provided by our H_2 lamp, it is likely a transition of a Rydberg series converging on the ground state of the cation.

Except for the transformation of **19** into **2**, intrinsic reaction coordinate (IRC) calculations starting from the crucial transition states (and following minimum energy paths down both sides of the saddle point) pertain to the ground singlet PES. Along the reaction paths, promotion to upper electronic states was introduced using vertical excitation. Species **19** is exceptional among the C_4H_3N isomers in that its ground electronic state has triplet multiplicity.[13] Our analysis indicates its special role in the photochemistry of **1**.

Following a singlet–singlet excitation, **1** may experience an intersystem crossing to a triplet surface and, if sufficient energy is available to overcome the barrier in T_1 (Fig. 7, column B) it may rearrange to **19T**. IRC calculations were further performed on the T_1 surface connecting **19T** to **2T** (note that while "T_0" would be appropriate for species **19**, the "T_1" label is used throughout for the sake of consistency). A molecule which previously crossed the barrier of at least 550 kJ mol^{-1} between **1** and **19** is energetic enough to reach the transition state (at approx. 400 kJ mol^{-1}, column D) leading from **19T** to **2T**.

Column E depicts the **2T** to **2S** path that completes the sequence photochemically transforming **1** into **2**. Calculations were

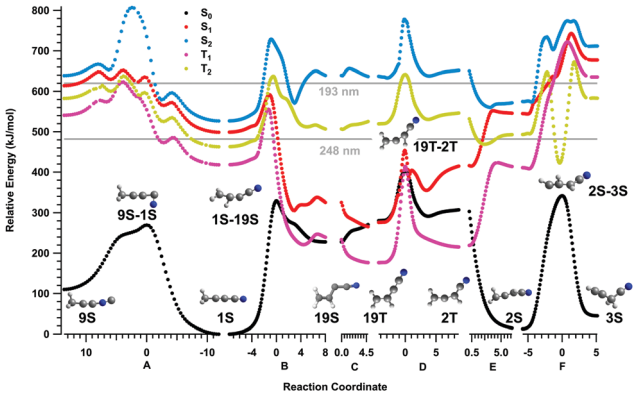

Fig. 7 Energies in ground and selected excited states during isomerization from **1** to **3** (columns B to F) and from **1** to **9** (column A). Excited state PESs energies calculated using TD DFT B1B95/aug-cc-pVTZ and assuming vertical transitions from IRC-derived S_0 (or T_1, for columns C and D) surfaces. Selected structures from each reaction coordinate are given here and in Fig. S78–S84, ESI.† Energies relative to predicted ground electronic state of **1**. Energies of UV sources applied in the photolysis experiments are indicated with the 121.6 nm source off scale (984 kJ mol^{-1}).

performed for the S_0 surface using the **2T** structure to start the IRC procedure, rather than a transition state. There is clearly an intersection between the S_0 and T_1 surfaces in the vicinity of the **2T** geometry, providing the expected relaxation towards **2S**. In addition to explaining the steps leading from **1** to **2**, this analysis helps to explain why the reverse process, **2** to **1**, was not detected. Following excitation of **2S**, some fraction of molecules may relax to the T_1 state. Efficient relaxation back to **2S** then follows, pre-empting any transformation towards **19**. Should the region around T_1 of **19** somehow be reached, there is a high barrier to conversion into **1** that further hinders this transformation. Conversion of **2** to **3** (see below) is also observed to be an efficient photochemical transformation and is preferred to the complicated path leading back to **1**.

Isomerization of 2 to 3. Column F of Fig. 7 illustrates the photochemical rearrangement from **2** to **3**. For this transformation, the IRC calculation once again proceeds from the saddle point on the ground singlet PES, and vertical excitations from the resultant structures are performed. Following absorption of a UV photon, the reaction can proceed provided that either the T_1 PES barrier at ~650 kJ mol^{-1} or the crossing between T_1 and S_1 at ~620 kJ mol^{-1} is reached. Much like the transformation from **1** to **2**, this channel is accessible for H_2 lamp radiation and possibly for the ArF laser at 620 kJ mol^{-1}, depending on the uncertainty of computations. Only two-photon absorption of the KrF radiation would be able to surmount this barrier. Once the barrier is cleared, a deep well exists on the triplet surface which approaches the S_0 surface at the transition state. This close approach allows relaxation onto the S_0 surface and the ensuing formation of either **2** or **3**. Considering the reverse process, **3** to **2**, which the kinetic model indicates as being more efficient, the DFT-predicted barrier to entry into the triplet-state well is slightly higher than from **2** or **3**. Such inequality is not reflected in the reaction rate coefficients, where $k_{23} < k_{32}$. This points to uncertainties in the experimental evaluation of these rate coefficients or in the DFT-derived saddle point energies.

Towards isocyanides. We did not observe any trace of isomer **9** during irradiation of **1**, a possible explanation for which can be seen in column A of Fig. 7. The energy of the lowest triplet state of **9** is much higher than that of **1**.[13] Even if the molecule reaches an isocyanide conformation by surmounting the barrier on an excited-state PES, it can easily transform back. Furthermore, for species **1**, the barrier involved in hydrogen migration (column B, T_1 surface) is lower than that for turning of the CN group (column A).

Just as for the **1**/**9** pair, the lowest triplet states of the isocyanides **6** and **10** are higher in energy than those of the respective cyanides **2** and **3**.[13] Overall, the formation of R-NC species is not a preferred photochemical process for **1**, **2**, or **3**.

Conclusions

Photolysis of Ar matrix isolated CH_3–C≡C–CN (**1**) at a variety of wavelengths produces CH_2=C=CH–CN (**2**) and H–C≡C–CH_2–CN (**3**) as the major products. A simple kinetic model explicitly involving these three most stable C_4H_3N-stoichometry molecules was proposed. Limited evidence for the formation of CH_2=C=CH–NC (**6**), H–C≡C–CH_2–NC (**10**), 3-cyanocyclopropene (**8**) and CH_2CCCNH (**4**) makes these identifications tentative. The observed lack of conversion between cyanopropyne and isocyanopropyne (**9**) is an exception to the general prevalence of this process observed to date in photolysis of similar carbon chain molecules in Ar matrices. These experimental results have been explained using a theoretical description of ground- and excited-state potential energy surfaces. Experimental searches for thus far unobserved cyanopropyne isomers, in particular the imine **4**, deserve revisiting.

Conflicts of interest

There are no conflicts to declare.

Acknowledgements

This study was supported with the funds of the Polish National Science Centre, projects No. 2011/03/B/ST4/02763 and 2015/17/B/ST4/03875, as well as by the French-Polish Polonium project (2015–2016, No. 33570RK). U. Szczepaniak is a beneficiary of the project ''Scholarships for PhD students of Podlaskie Voivodeship'' co-financed by the European Social Fund, Polish Government, and Podlaskie Voivodeship. T. Custer would like to acknowledge COST STSM action 39577 for providing funding for exchange between PIIM and Warsaw crucial to production of this work. J.-C. Guillemin thanks the Program PCMI (INSU-CNRS) and the Centre National d'Etudes Spatiales (CNES) for funding support.

References

1 N. W. Broten, J. M. Macleod, L. W. Avery, W. M. Irvine, B. Hoglund, P. Friberg and A. Hjalmarson, *Astrophys. J.*, 1984, **276**, L25–L29.
2 A. Belloche, H. S. P. Müller, K. M. Menten, P. Schilke and C. Comito, *Astron. Astrophys.*, 2013, 559.
3 V. Vuitton, R. V. Yelle and M. J. McEwan, *Icarus*, 2007, **191**, 722–742.
4 J. C. Loison, E. Hébrard, M. Dobrijevic, K. M. Hickson, F. Caralp, V. Hue, G. Gronoff, O. Venot and Y. Bénilan, *Icarus*, 2015, **247**, 218–247.
5 Y. n. Chin, R. I. Kaiser, C. Lemme and C. Henkel, *AIP Conf. Proc.*, 2006, **855**, 149–153.
6 F. J. Lovas, J. M. Hollis, A. J. Remijan and P. R. Jewell, *Astrophys. J.*, 2006, **645**, L137–L140.
7 D. K. Bohme and A. B. Raksit, *Mon. Not. R. Astron. Soc.*, 1985, **213**, 717–720.
8 M. J. McEwan, D. A. Fairley, G. B. I. Scott and V. G. Anicich, *J. Phys. Chem.*, 1996, **100**, 4032–4037.
9 G. Schwahn, G. Winnewisser, W. Joentgen, H. J. Altenbach and E. Vogel, *Astron. Astrophys.*, 1986, **161**, 327–328.
10 A. Singh, Shivani, A. Misra and P. Tandon, *Res. Astron. Astrophys.*, 2014, **14**, 275–284.
11 D. Quan and E. Herbst, *Astron. Astrophys.*, 2007, **474**, 521–527.
12 N. Balucani, O. Asvany, R. I. Kaiser and Y. Osamura, *J. Phys. Chem. A*, 2002, **106**, 4301–4311.
13 T. Custer, U. Szczepaniak, M. Gronowski, E. Fabisiewicz, I. Couturier-Tamburelli and R. Kolos, *J. Phys. Chem. A*, 2016, **120**, 5928–5938.
14 R. Tubino, G. Dellepia and G. Zerbi, *J. Chem. Phys.*, 1969, **50**, 621–627.
15 F. Cerceau, F. Raulin, R. Courtin and D. Gautier, *Icarus*, 1985, **62**, 207–220.
16 M. Khlifi and F. Raulin, *Spectrochim. Acta, Part A*, 1991, **47**, 171–176.
17 S. Torker, D. Kvaskoff and C. Wentrup, *J. Org. Chem.*, 2014, **79**, 1758–1770.
18 N. DelloRusso and R. K. Khanna, *Icarus*, 1996, **123**, 366–395.
19 P. Kurtz, H. Gold and H. Disselnkotter, *Justus Liebigs Ann. Chem.*, 1959, **624**, 1–25.
20 C. Wentrup and W. D. Crow, *Tetrahedron*, 1970, **26**, 4915–4924.
21 J. W. Zwikker and R. W. Stephany, *Synth. Commun.*, 1973, **3**, 19–23.
22 A. Chrostowska, A. Matrane, D. Maki, S. Khayar, H. Ushiki, A. Graciaa, L. Belachemi and J.-C. Guillemin, *ChemPhysChem*, 2012, **13**, 226–236.
23 A. Benidar, D. Begue, F. Richter, C. Pouchan, M. Lahcini and J.-C. Guillemin, *ChemPhysChem*, 2015, **16**, 848–854.
24 H. Møllendal, S. Samdal, A. Matrane and J. C. Guillemin, *J. Phys. Chem. A*, 2011, **115**, 7978–7983.
25 R. Kołos and J. Waluk, *J. Mol. Struct.*, 1997, **408**, 473–476.
26 R. L. Hudson and M. H. Moore, *Icarus*, 2004, **172**, 466–478.
27 A. Coupeaud, M. Turowski, M. Gronowski, N. Piétri, I. Couturier-Tamburelli, R. Kołos and J.-P. Aycard, *J. Chem. Phys.*, 2007, **126**, 164301.
28 A. M. Smith, G. Schallmoser, A. Thoma and V. E. Bondybey, *J. Chem. Phys.*, 1993, **98**, 1776–1785.
29 R. Kołos, *Chem. Phys. Lett.*, 1999, **299**, 247–251.
30 M. E. Jacox, *J. Mol. Spectrosc.*, 1978, **71**, 369–385.
31 D. E. Milligan and M. E. Jacox, *J. Chem. Phys.*, 1967, **47**, 278–285.
32 A. Toumi, I. Couturier-Tamburelli, T. Chiavassa and N. Piétri, *J. Phys. Chem. A*, 2014, **118**, 2453–2462.
33 H. Bürger, D. Lentz, B. Meisner, N. Nickelt, D. Preugschat and M. Senzlober, *Chem. – Eur. J.*, 2000, **6**, 3377–3385.
34 J. Gripp, A. Guarnieri, W. Stahl and D. Lentz, *J. Mol. Struct.*, 2000, **526**, 81–96.
35 F. Scappini, C. Codella and A. Guarnieri, *Mon. Not. R. Astron. Soc.*, 1996, **283**, L7–L8.
36 B. T. Hill and M. S. Platz, *Phys. Chem. Chem. Phys.*, 2003, **5**, 1051–1058.
37 C.-F. Su and M. D. Harmony, *J. Mol. Spectrosc.*, 1984, **108**, 58–65.
38 Y. Masuyama, Y. Ueno and M. Okawara, *Chem. Lett.*, 1977, **6**, 835–838.
39 K. Ohno and S. Maeda, *Phys. Scr.*, 2008, **78**, 1–8.
40 M. E. Jacox, *Chem. Phys.*, 1979, **43**, 157–172.
41 S. V. Kameneva, A. D. Volosatova and V. I. Feldman, *Radiat. Phys. Chem.*, 2017, **141**, 363–368.
42 B. McCarrol, *Rev. Sci. Instrum.*, 1970, **41**, 279–280.
43 N. F. W. Ligterink, D. M. Paardekooper, K.-J. Chuang, M. L. Both, G. A. Cruz-Diaz, J. H. van Helden and H. Linnartz, *Astron. Astrophys.*, 2015, **584**, A56.
44 A. Toumi, N. Piétri, T. Chiavassa and I. Couturier-Tamburelli, *Icarus*, 2016, **270**, 435–442.
45 A. D. Becke, *J. Chem. Phys.*, 1996, **104**, 1040.
46 C. T. Lee, W. T. Yang and R. G. Parr, *Phys. Rev. B: Condens. Matter Mater. Phys.*, 1988, **37**, 785.
47 R. A. Kendall, T. H. Dunning and R. J. Harrison, *J. Chem. Phys.*, 1992, **96**, 6796–6806.
48 R. L. Jacobsen, R. D. Johnson, K. K. Irikura and R. N. Kacker, *J. Chem. Theory Comput.*, 2013, **9**, 951–954.
49 C. Peng and H. B. Schlegel, *Isr. J. Chem.*, 1993, **33**, 449–454.
50 C. Peng, P. Y. Ayala, H. B. Schlegel and M. J. Frisch, *J. Comput. Chem.*, 1996, **17**, 49–56.
51 X. Li and M. J. Frisch, *J. Chem. Theory Comput.*, 2006, **2**, 835–839.
52 K. Fukui, *Acc. Chem. Res.*, 1981, **14**, 363–368.
53 A. R. Allouche, *J. Comput. Chem.*, 2011, **32**, 174–182.
54 A. D. Becke, *J. Chem. Phys.*, 1996, **104**, 1040–1046.
55 K. E. Riley, B. T. Op't Holt and K. M. Merz, Jr., *J. Chem. Theory Comput.*, 2007, **3**, 407–433.
56 Y. Zhao, J. Pu, B. J. Lynch and D. G. Truhlar, *Phys. Chem. Chem. Phys.*, 2004, **6**, 673.
57 M. Gronowski, *Comput. Theor. Chem.*, 2017, **1108**, 50–56.
58 L. Goerigk and S. Grimme, *Phys. Chem. Chem. Phys.*, 2011, **13**, 6670–6688.
59 R. Bauernschmitt and R. Ahlrichs, *Chem. Phys. Lett.*, 1996, **256**, 454–464.
60 M. E. Casida, C. Jamorski, K. C. Casida and D. R. Salahub, *J. Chem. Phys.*, 1998, **108**, 4439.

61 R. E. Stratmann, G. E. Scuseria and M. J. Frisch, *J. Chem. Phys.*, 1998, **109**, 8218.
62 A. Chantzis, A. D. Laurent, C. Adamo and D. Jacquemin, *J. Chem. Theory Comput.*, 2013, **9**, 4517–4525.
63 Y.-L. Wang and G.-S. Wu, *Int. J. Quantum Chem.*, 2008, **108**, 430–439.
64 R. M. Richard and J. M. Herbert, *J. Chem. Theory Comput.*, 2011, **7**, 1296–1306.
65 C.-P. Hsu, S. Hirata and M. Head-Gordon, *J. Phys. Chem. A*, 2001, **105**, 451–458.
66 F. Cordova, L. J. Doriol, A. Ipatov, M. E. Casida, C. Filippi and A. Vela, *J. Chem. Phys.*, 2007, **127**, 164111.
67 S. Chilukuri and W. L. Lichten, *Rev. Sci. Instrum.*, 1979, **50**, 256–257.
68 Y.-h. Ding, J.-l. Liu, X.-r. Huang, Z.-s. Li and C.-c. Sun, *J. Chem. Phys.*, 2001, **114**, 5170–5179.
69 A. Coupeaud, R. Kołos, I. Couturier-Tamburelli, J. P. Aycard and N. Piétri, *J. Phys. Chem. A*, 2006, **110**, 2371–2377.
70 A. D. Abbate and C. B. Moore, *J. Chem. Phys.*, 1985, **82**, 1255–1262.
71 K. Satoshi, M. Takayanagi and M. Nakata, *J. Mol. Struct.*, 1997, **413–414**, 365–369.
72 J. F. Ogilvie, S.-L. Chou, M.-Y. Lin and B.-M. Cheng, *Vib. Spectrosc.*, 2011, **57**, 196–206.
73 M. E. Jacox and D. E. Milligan, *Chem. Phys.*, 1974, **4**, 45–61.
74 A. V. Golovkin, D. I. Davlyatshin, A. L. Serebrennikova and L. V. Serebrennikov, *J. Mol. Struct.*, 2013, **1049**, 392–399.
75 K. V. J. Jose, S. R. Gadre, K. Sundararajan and K. S. Viswanathan, *J. Chem. Phys.*, 2007, **127**, 104501.
76 S. Ikuta, T. Tsuboi and K. Aoki, *THEOCHEM*, 2000, **528**, 297–305.
77 M. Z. Kassaee, S. Z. Sayyed-Alangi and Z. Hossaini, *THEOCHEM*, 2004, **676**, 7–14.
78 M. C. McCarthy, J. U. Grabow, M. J. Travers, W. Chen, C. A. Gottlieb and P. Thaddeus, *Astrophys. J.*, 1999, **513**, 305–310.
79 J. Y. Qi, M. D. Chen, W. Wu, Q. E. Zhang and C. T. Au, *Chem. Phys.*, 2009, **364**, 31–38.
80 K. M. Vogelhuber, S. W. Wren, C. J. Shaffer, R. J. McMahon, A. B. McCoy and W. C. Lineberger, *J. Chem. Phys.*, 2011, **135**, 204307.
81 M. E. Jacox, *J. Mol. Spectrosc.*, 1977, **66**, 272–287.
82 D. E. Milligan and M. E. Jacox, *J. Chem. Phys.*, 1967, **47**, 5146–5156.
83 J. Pacansky and J. Bargon, *J. Am. Chem. Soc.*, 1975, **97**, 6896–6897.
84 P. Bruston, H. Poncet, F. Raulin, C. Cossartmagos and R. Courtin, *Icarus*, 1989, **78**, 38–53.
85 N. Lamarre, C. Falvo, C. Alcaraz, B. Cunha de Miranda, S. Douin, A. Flütsch, C. Romanzin, J. C. Guillemin, S. Boyé-Péronne and B. Gans, *J. Mol. Spectrosc.*, 2015, **315**, 206–216.